

# Low-noise high-speed InGaAs/InP-based single-photon detector

Xiuliang Chen, E Wu, Guang Wu, and Heping Zeng\*

State Key Laboratory of Precision Spectroscopy, East China Normal University, Shanghai 200062, China

\*hpzeng@phy.ecnu.edu.cn

**Abstract:** A low-noise high-speed InGaAs/InP-based single-photon detector was demonstrated with a double-self-differencing spike signal cancellation technique. A photon-number resolving method was used to analyze the ratio of avalanche signal to background noise. By adding a post-self-differencing circuit to the pre-self-differencing circuit, the signal to noise ratio was improved by 11.0 dB. The typical error count probability was as low as 2.1% and 6.4% at the detection efficiency of 20.6% and 30.5%, respectively.

©2010 Optical Society of America

OCIS codes: (270.0270) Quantum optics; (040.0040) Detectors; (030.5260) Photon counting.

---

## References and links

1. C. H. Bennett, and G. Brassard, "Quantum cryptography: Public key distribution and coin tossing", in Proceedings of the IEEE international Conference on Computers, Systems and Signal Processing (Institute of Electrical and Electronics Engineers, New York, 1984), pp. 175–179.
2. X. F. Mo, B. Zhu, Z. F. Han, Y. Z. Gui, and G. C. Guo, "Faraday-Michelson system for quantum cryptography," *Opt. Lett.* **30**(19), 2632–2634 (2005).
3. K. Gordon, V. Fernandez, G. Buller, I. Rech, S. Cova, and P. Townsend, "Quantum key distribution system clocked at 2 GHz," *Opt. Express* **13**(8), 3015–3020 (2005).
4. C. Zhou, G. Wu, X. Chen, and H. Zeng, "Plug and play" quantum key distribution system with differential phase shift," *Appl. Phys. Lett.* **83**(9), 1692–1694 (2003).
5. P. Michler, A. Kiraz, C. Becher, W. V. Schoenfeld, P. M. Petroff, L. Zhang, E. Hu, and A. Imamoglu, "A quantum dot single-photon turnstile device," *Science* **290**(5500), 2282–2285 (2000).
6. A. Wehr, and U. Lohr, "Airborne laser scanning—an introduction and overview," *ISPRS J. Photogramm. Remote Sens.* **54**(2-3), 68–82 (1999).
7. T. Ioshima, Y. Isojima, K. Hakomori, K. Kikuchi, K. Nagai, and H. Nakagawa, "Ultrahigh sensitivity single-photon detector using a Si avalanche photodiode for the measurement of ultraweak bioluminescence," *Rev. Sci. Instrum.* **66**(4), 2922–2926 (1995).
8. A. Lacaita, F. Zappa, S. Cova, and P. Lovati, "Single-photon detection beyond 1  $\mu\text{m}$ : performance of commercially available InGaAs/InP detectors," *Appl. Opt.* **35**(16), 2986–2996 (1996).
9. A. Tomita, and K. Nakamura, "Balanced, gated-mode photon detector for quantum-bit discrimination at 1550 nm," *Opt. Lett.* **27**(20), 1827–1829 (2002).
10. D. S. Bethune, W. P. Risk, and G. W. Pabst, "A high-performance integrated single-photon detector for telecom wavelengths," *J. Mod. Opt.* **51**, 1359–1368 (2004).
11. N. Namekata, S. Sasamori, and S. Inoue, "800 MHz single-photon detection at 1550-nm using an InGaAs/InP avalanche photodiode operated with a sine wave gating," *Opt. Express* **14**(21), 10043–10049 (2006).
12. G. Ribordy, J. D. Gautier, H. Zbinden, and N. Gisin, "Performance of InGaAs/InP Avalanche Photodiodes as Gated-Mode Photon Counters," *Appl. Opt.* **37**(12), 2272–2277 (1998).
13. A. Tomita, and K. Nakamura, "Balanced, gated-mode photon detector for quantum-bit discrimination at 1550 nm," *Opt. Lett.* **27**(20), 1827–1829 (2002).
14. G. Wu, C. Zhou, X. Chen, and H. Zeng, "High performance of gated-mode single-photon detector at 1.55  $\mu\text{m}$ ," *Opt. Commun.* **265**(1), 126–131 (2006).
15. G. Wu, Y. Jian, E. Wu, and H. Zeng, "Photon-number-resolving detection based on InGaAs/InP avalanche photodiode in the sub-saturated mode," *Opt. Express* **17**(21), 18782–18787 (2009).
16. Z. L. Yuan, B. E. Kardynal, A. W. Sharpe, and A. J. Shields, "High speed single photon detection in the near infrared," *Appl. Phys. Lett.* **91**(4), 041114 (2007).
17. B. E. Kardynal, Z. L. Yuan, and A. J. Shields, "An avalanche-photodiode-based photon-number-resolving detector," *Nat. Photonics* **2**(7), 425–428 (2008).
18. L. Xu, E. Wu, X. Gu, Y. Jian, G. Wu, and H. Zeng, "High-speed InGaAs/InP-based single-photon detector with high efficiency," *Appl. Phys. Lett.* **94**(16), 161106 (2009).
19. X. Chen, E. Wu, L. Xu, Y. Liang, G. Wu, and H. Zeng, "Photon-number resolving performance of the InGaAs/InP avalanche photodiode with short gates," *Appl. Phys. Lett.* **95**(13), 131118 (2009).

## 1. Introduction

Single-photon detectors based on avalanche photodiodes (APDs) are widely used in quantum key distribution [1–4], quantum dot characterization [5], laser ranging [6] and bioluminescence detection [7]. In particular, single-photon detection at telecom wavelengths around 1300 and 1500 nm relies on InGaAs/InP APDs [8–11]. Typically, an InGaAs/InP APD operates in the gated Geiger mode [12], in which the bias voltage applied on the APD is maintained below the breakdown voltage and repetitive pulse series raise the voltage above the breakdown voltage for a short duration in each gating cycle. The avalanche is controlled by the gating pulse duration. As a photon arrives at the APD during the short gating period, a photocarrier is excited and an avalanche multiplication is triggered in the InP layer of the APD. At the falling edge of the gating pulse, the voltage applied on the APD falls below the breakdown voltage and the avalanche is quenched. However, the gating pulses may generate spike signals by charging and subsequent discharging on the capacitance of the APD, and weak avalanche signals are in general buried in the spike signals. When a discrimination level is set to separate the avalanche signal from the spike signal, the avalanche signal whose peak output voltage is lower than the peak voltage of the spike signal cannot be recognized as a valid detectable photon count. Therefore, the detection efficiency is typically lower than the ideal quantum efficiency of the APD. In the conventional gated Geiger mode, the avalanche gain of the APD is usually set very high in order to achieve efficient discrimination and hence increase the detection efficiency, causing the avalanche multiplication of the APD to be instantaneously saturated. On the other hand, the detection rate of the APD is limited to a few MHz due to the detrimental influence of the high dark noise and afterpulse probability.

If the spike signal could be suppressed down to a sufficiently low level, weak single-photon clicks could be discriminated from the background or electronic noise at a reduced discrimination level, an observable increase of the detection efficiency may be achieved, and the APD may even operate in the non-saturated avalanche mode for the photon-number-resolving detection. Spike signals could be cancelled by using a coaxial cable reflection line [10], a hybrid junction to balance the outputs of two APDs [13] or the outputs of an APD and a compensating diode [14], and optical balancing technique [15]. As these methods developing, the maximum detection efficiency was up to 30%, and the dark count was as low as  $10^{-6}$ . Recently, Yuan et al. introduced a robust self-differencing technique to cancel spike signals on the basis of subtracting the identical signal in the APD response of the two successive gating cycles [16–19]. By using this technique, the spike signal was suppressed to a quite low level, and small avalanche signals buried in the non-suppressed spike signals could be extracted at a low discrimination level. As a consequence, the same detection efficiency could be maintained with a low avalanche multiplication. The APD could operate with dramatically decreased dark count and afterpulse noise, and hence the single-photon detection speed could increase up to gigahertz [16, 17]. By using the self-differencing technique, the maximum detection efficiency can be up to 29.3% with the error count probability of 6%. As the spike noise was suppressed, the avalanche signal could be directly measured in the non-saturated avalanche mode. A photon-number resolving detection could be achieved by analyzing the distribution of the peak output of the avalanche signal [17, 19].

In this paper, we present the experimental demonstration of a double-self-differencing technique for spike signal cancellation to further improve the ratio of the avalanche signal to noise. By adding a post-self-differencing circuit to the pre-self-differencing circuit in the spike-cancellation module, the average voltage of the single-photon click at the InGaAs/InP APD was increased while the background electronic noise was further suppressed. As analyzed by the photon-number resolving method, the ratio of avalanche signal to background noise was improved up to 17.5 dB, which enabled a distinct discrimination of weak avalanche signals conventionally buried in the non-suppressed spike signals and electronic noise and thus facilitated an increase of the detection efficiency with the same incident photon flux. The performance of the double-self-differencing single-photon detector was characterized with the gating pulse duration of 700 ps at  $-30^{\circ}\text{C}$  at the fixed gating frequency of 200 MHz. The error

count probability was as low as 2.1% and 6.4%, when the detection efficiency was 20.6% and 30.5%, respectively.

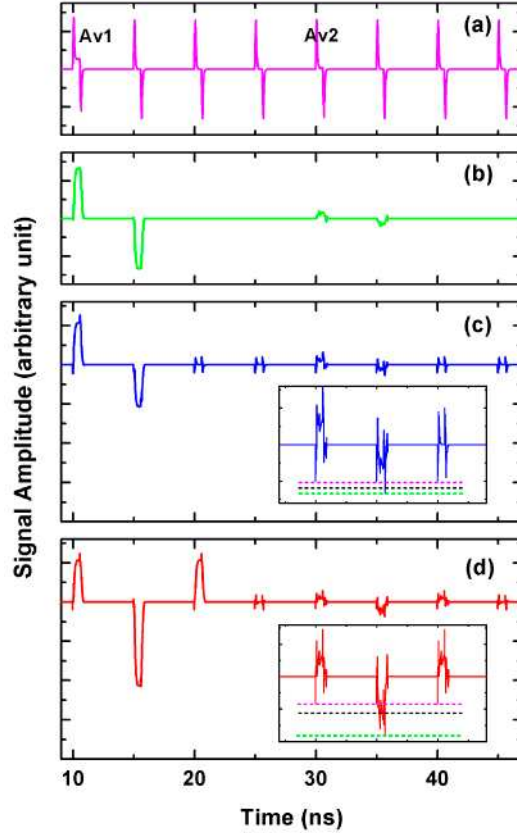


Fig. 1. Simulated waveforms in the double-self-differencing module. (a) Response of the APD in eight cycles with a strong and a weak avalanche at the 1st and 5th cycle, respectively. Av1: a strong avalanche at the 1st cycle; Av2: a weak avalanche at the 5th cycle. (b) Subtracted spike and avalanche signals after the pre-self-differencing with exact self-differencing delay to match the repetitive cycles. (c) Weak avalanche signal buried in the incompletely suppressed spike signal as the self-differencing delay is mismatched by 2 ps to the repetitive cycles; Inset: enlarged view of weak avalanche signal buried in the incompletely suppressed spike signal. (d) Further suppressed spike and increased avalanche signals after the double-self-differencing process. Inset: enlarged view of weak avalanche after double-self-differencing process. The pink, black and green dashed lines in the insets of (c) and (d) are the level of the peak voltage of the background noise, the discrimination level and the peak voltage of the avalanche signal, respectively.

## 2. Principle of double-self-differencing module

Figure 1 shows the simulated waveforms in the double-self-differencing module. Figure 1(a) plots the response of the APD in eight cycles. Assume that there are a strong and a weak avalanche signals at the 1st and 5th cycles, respectively. The avalanche output of the APD is firstly subtracted from the same output of APD delayed by  $\Delta t_1$ . After subtracting, the subtracted spike and avalanche signals can be expressed by

$$V_{pre-sup}(t) = a[V_{ss}(t) - V_{ss}(t - \Delta t_1)], \quad (1)$$

$$V_{pre-sig}(t) = a[V_{as}(t) - V_{as}(t - \Delta t_1)], \quad (2)$$

where  $V_{ss}(t)$  and  $V_{as}(t)$  denote the original spike signal and avalanche signal of the APD, respectively. And  $a$  is the scale factor in this process. As the spike signal is generated by the gating pulse, the spike signal  $V_{ss}(t)$  is a repetitive signal with the same frequency as the gating pulse. When the  $\Delta t_1$  is set to one gating pulse period, the spike signal could be suppressed, and the avalanche signal is converted to a positive part  $V_{as}(t)$  followed with a negative part  $-V_{as}(t-\Delta t_1)$ . In principle, all the spike signal could be completely suppressed, and the avalanche signal  $V_{pre-sig}(t)$  could be picked out easily, as shown in Fig. 1(b).

However, the spike signal is nevertheless difficult to be completely removed in practice mainly due to the technical difficulty in setting the self-differencing delay  $\Delta t_1$  exactly the same as the gating pulse period. Accordingly, some weak avalanche signals are still buried in the suppressed spike signal. Figure 1(c) shows the output of the pre-self-differencing detector for a self-differencing delay  $\Delta t_1$  mismatched to the gating pulse period by 2 ps. Due to incomplete suppression of the spike signal, the weak avalanche signal at the 5th cycle cannot be discriminated directly from the suppressed spike signal.

As the suppressed spike signal is also a repetitive signal with the same frequency, a post-self-differencing process could be added to further suppress the spike signal. The spike signal and avalanche signal after the second self-differencing process can be expressed as

$$V_{post-sup}(t) = b[V_{pre-sup}(t) - V_{pre-sup}(t - \Delta t_2)], \quad (3)$$

$$V_{post-sig}(t) = ab[V_{as}(t - \Delta t_1 - \Delta t_2) + V_{as}(t) - V_{as}(t - \Delta t_1) - V_{as}(t - \Delta t_2)], \quad (4)$$

where  $b$  is the scale factor of the post-self-differencing process and the  $\Delta t_2$  is the relative delay. As the self-differencing delays  $\Delta t_1$  and  $\Delta t_2$  are almost the same as the gating pulse duration, the spike signal is suppressed again, and the avalanche signal in the post-self-differencing process is converted to two positive signals [ $V_{as}(t)$  and  $V_{as}(t-\Delta t_1-\Delta t_2)$ ] at different times ( $t$  and  $t-\Delta t_1-\Delta t_2$ ) and one negative signal  $-V_{as}(t-\Delta t_1)-V_{as}(t-\Delta t_2)$  at the time  $t-\Delta t_1 \sim t-\Delta t_2$ . It is interesting to note that the negative signal has an amplitude almost twice of the positive peaks, as shown in Fig. 1(d). In comparison with the output waveforms of the pre-self-differencing process in Fig. 1(c), the negative peak of the weak avalanche signal in the 5th cycle is increased while the spike signal is suppressed further, and it can be discriminated. Thus, more avalanche signal can be picked out at the same photon clicks by using the double-self-differencing process. As Eq. (4) expresses, if there are avalanche events in the 1st, 2nd and 3rd cycles with almost the same avalanche signal amplitude, the avalanche signal after the post-self-differencing process would change to two positive signals and two negative signals. The two negative signals were corresponding to the avalanche events in the 1st and 3rd cycles, and the avalanche signal in the second would be counteracted with the avalanche signal in the first and third cycles. Due to the counteracted with the 2nd avalanche signal, the amplitude of the two negative signals was almost same as the positive signal.

### 3. Experimental setup

Figure 2 schematically shows the experimental setup of the single-photon detector by using the double-self-differencing technique. The InGaAs/InP APD (JDSU EXT 40-X00408052-005) was operated in the gated mode with a fixed gating pulse frequency of 200 MHz and gating pulse duration of 700 ps. Figure 3(a) shows the waveform of the amplified signal from the APD. The positive and negative peaks in the waveform came from the capacitance responses on the APD to the gating pulses, and the avalanche signal was buried in the spike signal. The response of the APD was then coupled to the spike-cancellation module consisting of the pre-self-differencing and post-self-differencing circuits. Each self-differencing circuit was composed of a 50/50 power splitter, a 180-degree power combiner and an amplifier. The original avalanche signal was divided into two identical components by the power splitter. After passing through two coaxial cables with different lengths, the pulse signal from the longer arm was delayed one gating pulse period, the same as in the original self-differencing scheme [16]. Then, the two components were combined again in the 180-degree power

combiner. The subtracting operation of the 180-degree power combiner extracts the avalanche signal from the spike noise. As shown in Fig. 3(b), the spike signal was suppressed, and the avalanche signal appeared as a positive peak and a following negative peak, which were contributed by the avalanche signal from the short and long coaxial cables, respectively.

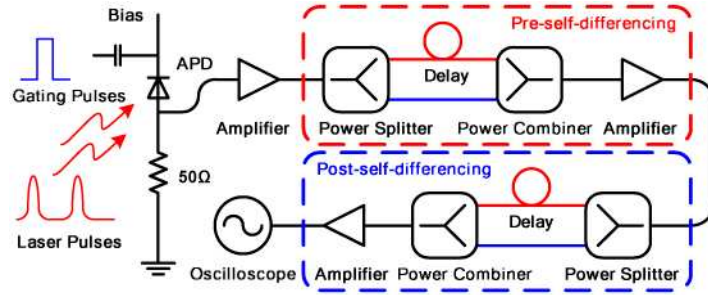


Fig. 2. Experimental setup of the double-self-differencing single-photon detector.

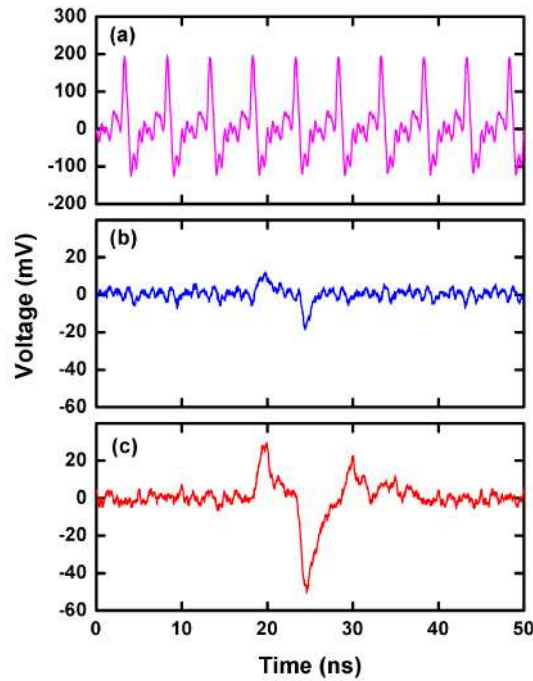


Fig. 3. Waveforms captured by an oscilloscope in the double-self-differencing single-photon detector. (a) Amplified APD response. (b) Output signal of the pre-self-differencing circuit. (c) Output signal of the post-self-differencing circuit.

The output signal from the pre-self-differencing circuit was then coupled to the post-self-differencing circuit. The setup of the post-self-differencing circuit was exactly the same as the pre-self-differencing circuit. After splitting and re-combining the signal in the post-self-differencing circuit, only the difference between the output signal of pre-self-differencing circuit from the long coaxial cable and the signal from the short coaxial cable was left, and the avalanche signal was changed to two small positive peaks and one large negative peak at the output of the post-self-differencing circuit as shown in Fig. 3(c). Because the background noise caused by mismatching of two coaxial cables in pre-self-differencing circuit was also a repeated signal with the same repetition frequency as the gating pulse frequency, the background noise was suppressed again. Meanwhile, the avalanche signal from the pre-self-

differencing circuit was amplified and re-combined in the post-self-differencing circuit. Thus, weak avalanche signal can be discriminated easily with an improved signal to noise ratio.

In our experiment, a 1.55- $\mu\text{m}$  pulsed laser diode with 19 ps pulse duration was synchronously triggered at 1/200 of the gating frequency. After attenuated, the photon pulse was coupled into the APD fiber pigtail as the photon source. The operation temperature of the APD was set to  $-30^\circ\text{C}$ . After passing through the pre-self-differencing and post-self-differencing circuits, the output signal was captured by an oscilloscope (6-GHz, Tektronix).

#### 4. Experimental results and discussion

As the amplitude of the avalanche signal was varied randomly, it was difficult to analyze the ratio of the avalanche signal to noise. For this reason, in our experiment, the photon-number resolving method was used to analyze the signal to noise ratio of the avalanche signal. Because the single-photon pulse used in the experiment was attenuated from a coherent light source, the probability of the peak output voltage of the avalanche signal could be considered as the superposition of different photon-number states [17, 19]. The average voltages of 0-photon and 1-photon states could be respectively considered as the average voltages of background noise and 1-photon-excited avalanche signal, and the signal to noise ratio could be directly calculated from the average voltages of the 0-photon and 1-photon states.

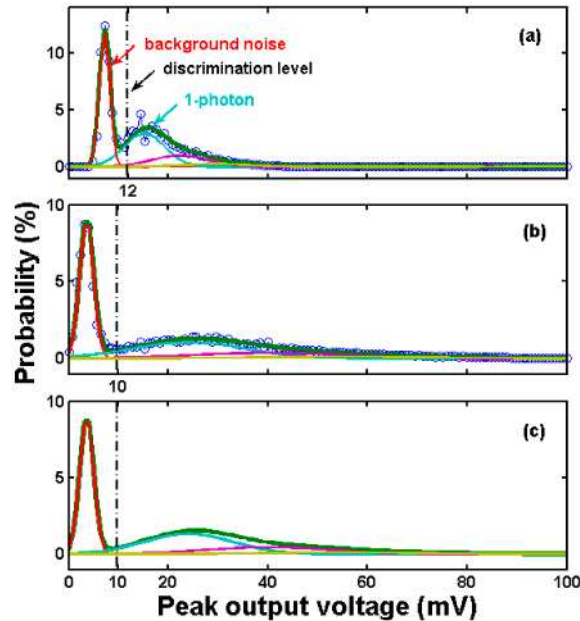


Fig. 4. Comparison of avalanche peak voltage distribution for (a) the pre-self-differencing and (b) double-self-differencing detector, respectively. (c) Simulated distribution of the double-self-differencing detector. The green solid line shows the simulations of the experiment data, and the red and blue solid lines present the background noise and 1-photon signal.

Figure 4 compares the typical distribution of the peak output voltages of the pre-self-differencing and double-self-differencing detectors. In both cases, the bias voltage was set to 55.0 V and the average detected photon number was kept less than 1 photon per pulse. By adding post-self-differencing to the pre-self-differencing, the average voltage of the 1-photon state increased to 24.0 mV while the background noise decreased to 3.2 mV. The signal to noise ratio characterized by comparing these two average voltages showed an improvement of 11.0 dB, from 6.5 dB to 17.5 dB. Figure 4(c) shows the simulated avalanche peak voltage distribution of the double-self-differencing detector by assuming a flat frequency response and negligible electronic noise in the post-self-differencing circuit. The real standard deviation of the 1-photon avalanche voltage was nevertheless larger than that calculated

directly by multiplying the scale factor of the post-self-differencing circuit due to the circuit noise and the non-flat frequency response.

Table 1 lists the avalanche probability of both pre-self-differencing and double-self-differencing circuits, which was calculated from Fig. 4. The ideal avalanche probability was the sum of all non-zero-photon states, which includes all the avalanche signal no matter whether it can be separated from the background noise or not. Since both measurements were kept under the same experimental condition and with the same quantum efficiency of the APD, the ideal avalanche probabilities were almost the same in the two measurements. The little difference between the ideal avalanche probabilities might be caused by the fluctuation of the bias voltage, the gating pulse duration, or the operation temperature of APD. However, in practice, we cannot detect all the avalanches, as a discrimination level was used to separate the background noise and the avalanche signal. According to the voltage distributions of the background noise, the discrimination levels of pre-self-differencing and double-self-differencing circuits were set to 12 and 10 mV, and the corresponding detected avalanche probability was 51.3% and 57.7%, respectively. The avalanche discrimination ability can be characterized by the ratio of the detected avalanche probability to the ideal avalanche probability. By adding the post-self-differencing circuit, the ratio was increased from 83.1% to 94.4%. This clearly indicated that the double-self-differencing circuit could improve the avalanche discrimination ability of the single-photon detector. It could be further improved by reducing the electronic noise and flattening the frequency response of the post-self-differencing circuit. The ideal ratio could be increased up to 96.5% according to the simulation shown in Fig. 4(c).

**Table 1. The ideal avalanche probability and detected avalanche probability of both pre-self-differencing and post-self-differencing circuits.**

	Ideal avalanche probability ( $P_{\text{ideal}}$ )	Discrimination level (mV)	Detected avalanche probability ( $P_{\text{detect}}$ )	$P_{\text{detect}}/P_{\text{ideal}}$
Pre-self-differencing	61.7%	12	51.3%	83.1%
Post-self-differencing	61.1%	10	57.7%	94.4%
Ideal post-self-differencing	61.6%	10	59.4%	96.5%

We next characterized the performance of the double-self-differencing single-photon detector and compared it with that of the pre-self-differencing detector. The incident photon pulse was attenuated to contain 1 photon per pulse on average before coupling into the APD. Figure 5(a) shows the detection efficiency as a function of the bias voltage. As the bias voltage increased, the detection efficiency of the double-self-differencing single-photon detector was up to 32%. Since the post-self-differencing circuit helped to discriminate the weak avalanche signal from the background noise, the detection efficiency of the double-self-differencing circuit was higher than that of the pre-self-differencing circuit. As shown in Fig. 5(a), the distinct difference of the detection efficiency was observed as the bias voltage on the APD was set for the detection efficiency below 20%. As the bias voltage was increased for a higher detection efficiency, the pre-self-differencing and double-self-differencing circuits exhibited less distinct difference of detection efficiency. This was caused by the fact that the amplitude of avalanche signal was increased with the detection efficiency, and less amount of avalanche was buried in the background noise.

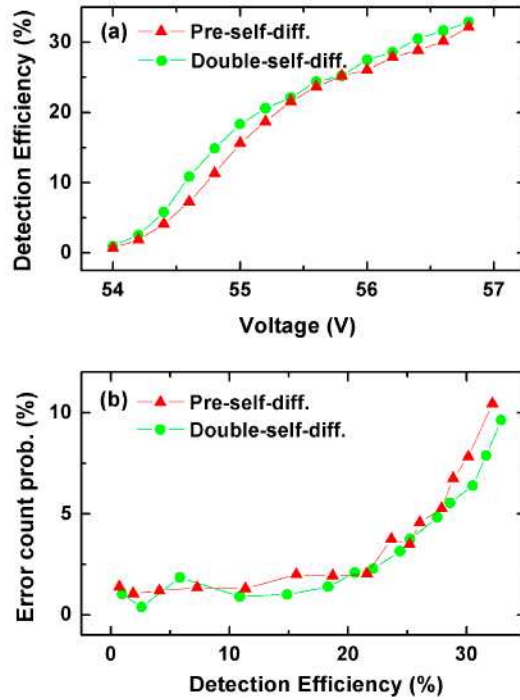


Fig. 5. (a) Detection efficiency as a function of the bias voltage. (b) Error count probability as a function of the detection efficiency.

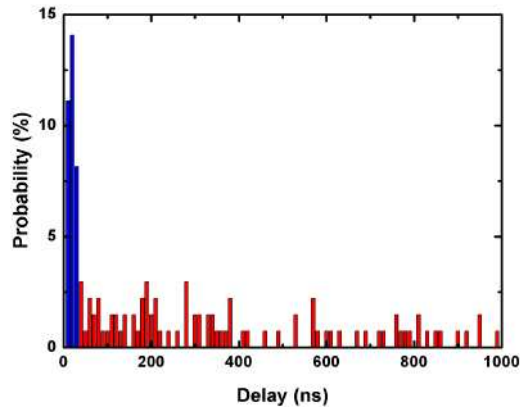


Fig. 6. Distribution of the afterpulse as a function of the delay time after the photon-excited avalanche.

As the incident photon pulse was synchronously triggered at  $1/200$  of gating pulse frequency, only the avalanches at the illuminated gating pulse contributed to the photon-excited signals, while the avalanches after the photon-excited avalanches originated in afterpulse and all the avalanches occurred at the non-illuminated gating pulses were regarded as error counts (including the dark count and afterpulse). Figure 6 presents the distribution of the afterpulse as a function of the delay time after the photon-excited avalanche. It shows that 33.3% of the afterpulse (the blue bars in Fig. 6) occurred in the first 30 ns after the photon-excited avalanche. Therefore, a 30-ns “count-off time” was applied in the experiment, i.e., avalanche occurred in the count-off time after the photon-excited avalanche was not counted. Figure 5(b) shows the error count probability as a function of the detection efficiency for the

pre-self-differencing and double-self-differencing single-photon detectors. In calculating the error count probability, we included the dark count and the afterpulse as the whole error counts. The error count probability  $P_e$  can be obtained by  $P_e = N_{all} / N_{ph} - 1$ , where  $N_{all}$  is the total counts at both illuminated and non-illuminated pulsing gates, and  $N_{ph}$  is the counts at illuminated pulse gates. As shown in Fig. 5(b), when the detection efficiency was between 10% and 20%, the error count probability of the double-self-differencing detector was lower than that of the pre-self-differencing detector. This shows a good agreement with difference of the detection efficiency in Fig. 4(a), because the detection efficiency of the double-self-differencing detector was much higher than that of pre-self-differencing detector when the detection efficiency was in the range from 10% to 20%. When the detection efficiency was 20.6%, the dark count probability and the error count probability were  $1.7 \times 10^{-5}$  and 2.1%. And the dark count probability and the error count probability were lowered to  $4.7 \times 10^{-5}$  and 6.4% at the detection efficiency of 30.5%. As the spike signal was deeply suppressed, the discrimination level was lowered and the small avalanche signal triggered by dark current may also be picked out to increase the dark count error. However, by using the double-differencing method, lots of tiny photon-excited avalanche signals survived in the discrimination process due to the lowered threshold voltage. As a result, the detection efficiency was much increased. Considering these two factors, the ratio of the dark count probability to the detection efficiency was decreased.

## 5. Conclusions

In conclusion, a low-noise high-speed InGaAs/InP-based single-photon detector was demonstrated with a double-self-differencing spike signal cancellation technique. The spike signal caused by the capacitance response of the APD was suppressed by adding a post-self-differencing circuit to the pre-self-differencing circuit. The avalanche signal to noise ratio was improved by 11.0 dB. The avalanche discrimination ability was improved and the detection efficiency was increased by using the double-self-differencing module at the same bias voltage. The error count probability of this single-photon detector was reduced to 2.1% and 6.4% at the detection efficiency of 20.6% and 30.5%, respectively.

## Acknowledgement

This work was funded in part by National Natural Science Fund of China (10990101, 10525416, 107740445 & 10904039), National Key Project for Basic Research (2006CB921105), Projects from Shanghai Science and Technology Commission (8530708200 & 08dz1400703), and Shanghai Leading Academic Discipline Project (B408).